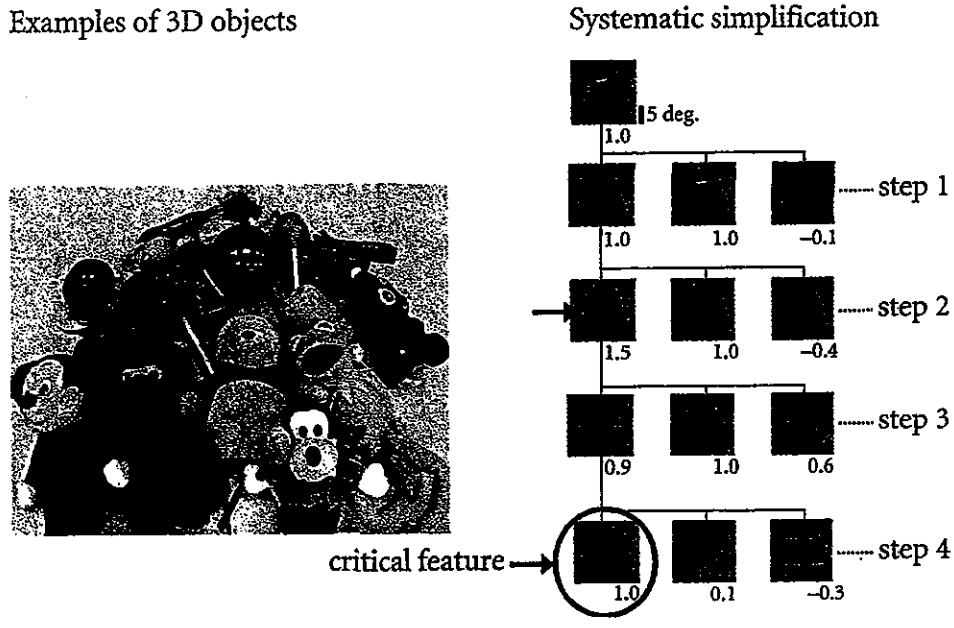

Fig. 12.1 The 'critical feature', the visual feature that maximally activates each cell, is determined by systematic stimulus simplification of the best object stimulus. First, we tested the cell with various three-dimensional objects, including faces, hands, stuffed animals, plastic fruits and vegetables, and paper mounts (left panel for some examples). After determining the best stimulus, we simplified it step by step to find the simplest stimulus that maximally activates the cell (right panel). For example, at step 1, we compared the best coloured object with its silhouette, and found that the silhouette activated the cell equally well. The rightmost rectangle was taken as a control stimulus. The numbers below each picture indicate the response amplitudes normalized to the response to the reference stimulus, the best object. The stimulus that evoked at least more than 70% of the response elicited by the best stimulus in the previous step, was *again* examined in the next step as the reference stimulus. At step 2, we examined the effect of the 'sharpness' of the corner at the junction of upper and lower parts (arrow), and found that the silhouette with the sharp corners was the most effective stimulus. From left to right, the stimuli were the silhouette with sharp corners, the silhouette that evoked the best response at the previous step, the silhouette without corners. Further simplification was carried out at step 3. Finally, we determined the critical feature as a combination of a circle and a rectangle because neither the upper nor lower part alone activated the cell.

visual stimuli that became familiar through training (Logothetis *et al.* 1995; Kobatake *et al.* 1998). The relationship between these neurons and those responding to visual features is also an issue that needs to be investigated.

Recently, intrinsic signal imaging has enabled us to reveal the spatial distribution of neurons activated by object images and to investigate response properties of neurons in characteristic sites revealed by intrinsic signal imaging. By this new approach, we have begun to understand more about object representation in area TE.

12.2 Intrinsic signal imaging

Neurons with similar response properties are clustered into a column in area TE (Gochin *et al.* 1991; Fujita *et al.* 1992). Thus, intrinsic signal imaging of columnar activation can be used to investigate spatial patterns of activation (Wang *et al.* 1996, 1998; Tsunoda *et al.* 2001). Intrinsic signal imaging measures the decrease in the degree of light reflection elicited by neural activation from the exposed cortical surface using a CCD camera (Fig. 12.2) (Grinvald *et al.* 1999). These reflection changes are due to metabolic changes elicited by neural activation, including deoxygenation of hemoglobin in capillaries (Grinvald *et al.* 1999).

Intrinsic signal imaging in area TE revealed multiple spots elicited by visual stimulation. The mean size of the 'active spots' (Fig. 12.2d) was 0.50 ± 0.13 mm along the longer axis and 0.35 ± 0.09 mm along the shorter axis ($n = 94$). These dimensions agreed well with the size previously reported for a column of cells with similar responsiveness in this area (Gochin *et al.* 1991; Fujita *et al.* 1992). Although these reflection changes are not a direct measure of neural activation, intrinsic signals coincide well with the activity of neurons examined by conventional extracellular recordings (Fig. 12.3) (Tsunoda *et al.* 2001).

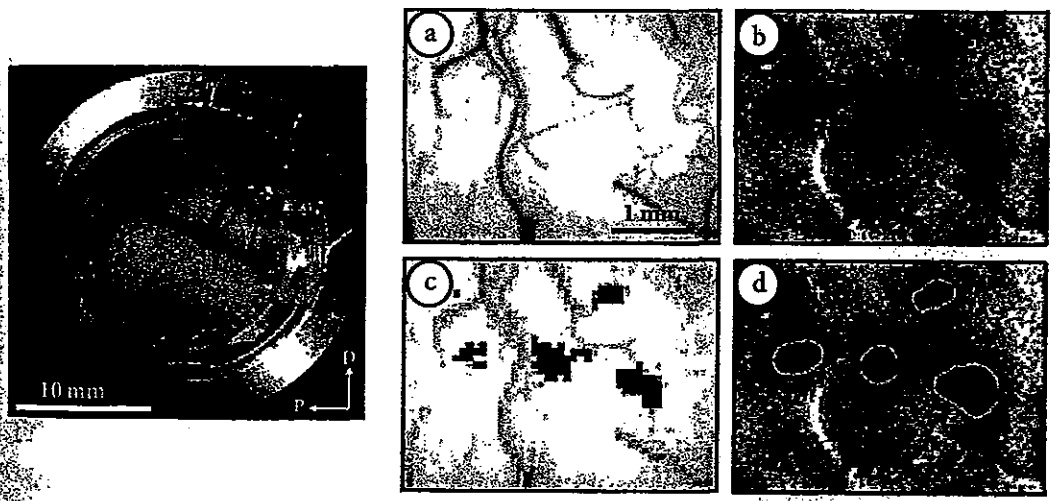

Fig. 12.2 Intrinsic signal imaging detects local modulation of light absorption changes in area TE. Surface view of the exposed portion of dorsal area TE (left panel). The thickest vessel running obliquely from the upper left to the lower right is along the superior temporal sulcus. The dorsal part of area TE is ventral to this vessel. (a) Portion of area TE where intrinsic signals were recorded. (b) A differential image showing a local increase in absorption. (c) Active regions, where the degree of reflection change evoked by the stimulus was significantly greater than that without the stimulus presentation. The region with the highest significance level is in red, that with the lowest significant level in yellow ($P < 0.05$). (d) Extracted active spots outlined by connecting pixels with 1/2 of the peak absorption value. (Modified from Tsunoda *et al.* 2001.)

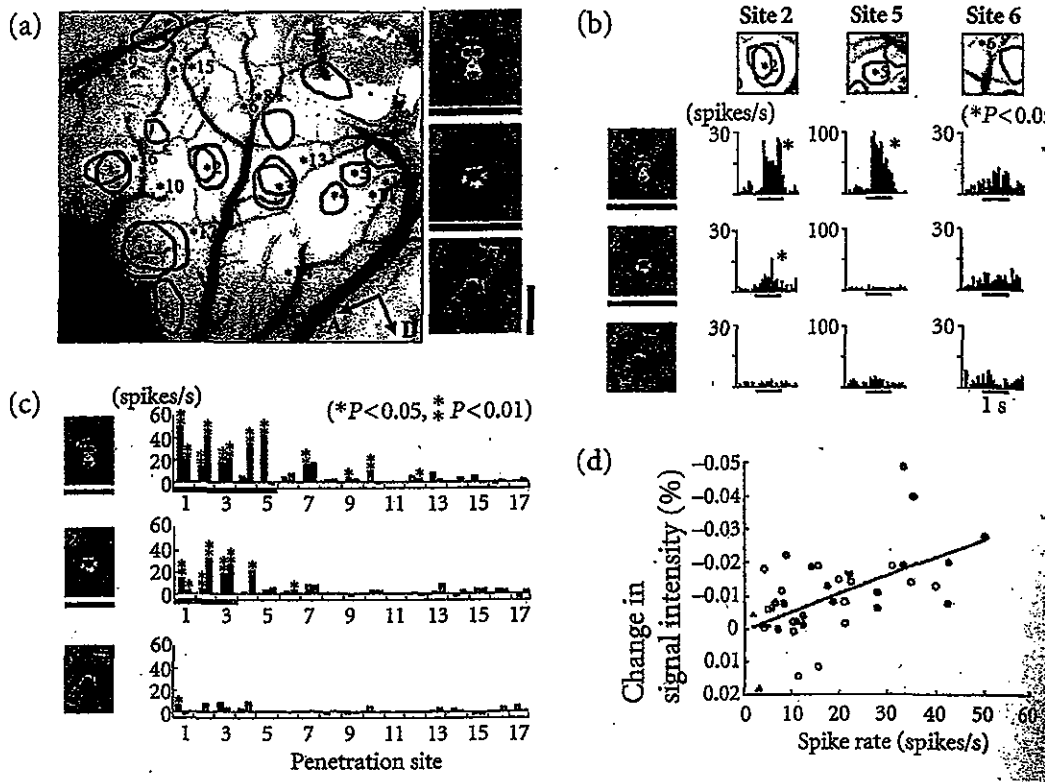

Fig. 12.3 Relationship between intrinsic signals and spike activity in area TE. (a) Active spots elicited by three different stimuli (*1*, *2* and *3*, on the right), and numbered electrode penetration sites. The color of individual contours indicates the active spots elicited by the stimulus underlined with the same color (same in all the figures showing spot distribution). A, anterior; D, dorsal. (b) Representative peristimulus–time histograms (PSTHs) showing the extracellular activity elicited by the three different stimuli, recorded at the sites indicated at the top of each column. Each row gives the PSTHs obtained following stimulation shown on the left side. Horizontal bars in the histograms indicate the one-second period for visual stimulation. (c) Mean firing rates evoked by the three different visual stimuli, for all 34 cells from 17 different sites. Two different cells separated by at least 200 μm were recorded at each penetration site. The penetration sites inside the active spots for a given stimulus were indicated by the colored bars in the top (red) and the second graphs (green). For stimulus 3, all the cells were recorded outside the active spot. (d) Correlation between the intensity of local changes of optical signal and evoked spike rates measured at the same cortical locations. Thirty-four cells were tested with 10 stimuli, and cellular activity with significant visual responses ($P < 0.05$) was plotted against the optical signal intensity obtained at the corresponding penetration sites for the individual stimuli. The activities of neurons from the same site were averaged. Different symbols indicate the responses at different sites. The regression line is given by $Y = -5.05e-6 + 5.46e-6X$ with a correlation coefficient of 0.57 ($n = 41$). Calibration bar, 10 degrees for the stimulus size in (a). Significance of difference determined by the Kolmogorov–Smirnov test for individual cell response is indicated by single ($P < 0.05$) or double ($P < 0.01$) asterisks in (b) and (c). (The same as in Fig. 12.5.) (Adapted from Tsunoda *et al.* 2001.)

To relate the optical response specificity to the neural activities, we recorded extracellular activity from 34 neurons in 17 sites located inside and outside the active spots (Fig. 12.3a). The representative peristimulus–time histograms (PSTHs) showed that the neuron in site 2, where both stimulus *1* and *2* elicited significant intrinsic signals, was activated by these two stimuli, but not by stimulus *3* (Fig. 12.3b, left-hand column). Similarly, only stimulus *1* significantly activated the cell in site 5 (Fig. 12.3b, middle column) and none of the stimuli activated cells in site 6 (Fig. 12.3b, right-hand column). In summary, among 34 neurons, 28 cells (82.4%) showed the same responsiveness to stimulus *1* as indicated by the optical responses: eight active cells inside the spot and twenty inactive cells outside (top row) (Fig. 12.3c). Similar results were obtained for 32 out of 34 cells (94.1%) for stimulus *2* (second row), and for 33 out of 34 cells (97.1%) for stimulus *3* (bottom row). A large variation of neuronal responses within the active spots (ex. Fig. 12.3c) did not alter the agreement between the intrinsic signals and extracellular responses. First, the optical response intensity and the firing rates of individual neurons showed a statistically significant positive correlation ($P < 0.001$) (Fig. 12.3d). Secondly, the average extracellular responses inside the spots (24.9 ± 17.2 and 16.8 ± 11.6 spikes/s for stimuli *1* and *2*, respectively) were significantly larger than those outside the spots (4.30 ± 4.95 and 3.32 ± 4.72 spikes/s for stimuli *1* and *2*, respectively) (Fig. 12.3c). These results indicate that the intrinsic signal coincides well with the firing activity of neurons examined by conventional extracellular recordings.

It should be mentioned that, in all the extracellular recordings, we recorded extracellular responses from superficial layers of cortex that are less than 1 mm in depth. Thus, strictly speaking, an 'active spot' revealed by intrinsic signal imaging may not necessarily correspond to a 'column', which usually means a cluster of neurons with similar response properties extending vertically from surface to the white matter. In the following sections, we use 'spots' for our results obtained by intrinsic signal imaging and 'columns' when we interpret our result in relation to previous studies.

12.3 Object representations revealed by intrinsic signal imaging

Intrinsic signal imaging revealed that different complex objects activated spots with different distribution patterns, together with some common active spots (Fig. 12.3a). Assuming that each spot represented a particular visual feature, the spots activated by one object may represent visual features specific to that object, and the spots activated by multiple objects may represent features common among these objects. We examined this idea by comparing distribution patterns of active spots with those produced by systematically simplified stimuli (Fig. 12.4) (Tsunoda *et al.* 2001). For example, in one case, a 'black cat' (a, *1*) was simplified to its 'head' (a, *2*), and then to the 'silhouette of a head' (a, *3*) (Fig. 12.4a). The original image (a, *1*) elicited 14 spots, but presenting only 'head' (a, *2*) elicited only eight of the original 14 spots. The silhouette (a, *3*) only activated three (yellow) of the eight spots elicited by the head (a, *2*). Similarly, Fig. 12.4b shows that spots A and B disappeared but spot D remained when the 'handle' and

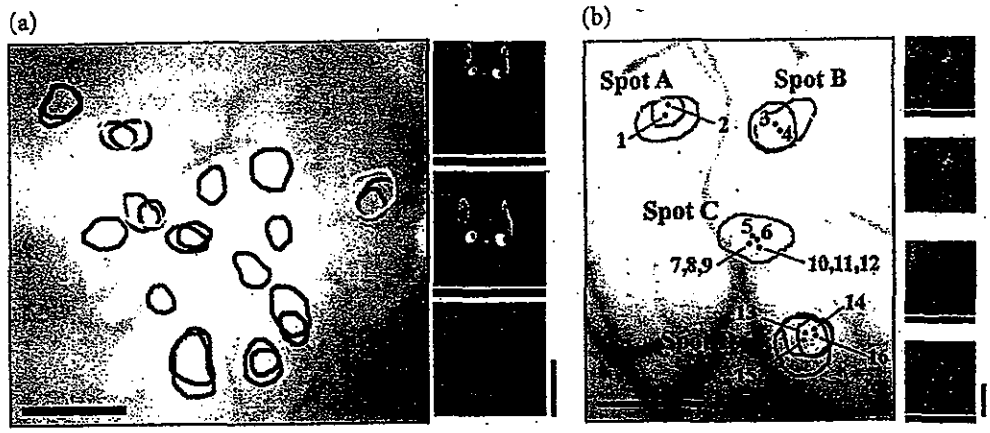

Fig. 12.4 Representation of complex object images and their simplification in area TE. (a) A case where simplified stimuli elicited only a subset of spots evoked by more complex stimuli. (b) Cases in which new spots appeared when the original stimulus was simplified. The numbers (1–16) indicate electrode penetration sites. (Modified from Tsunoda *et al.* 2001.)

'hose' were removed from the original stimulus, 'fire extinguisher'. In addition to the disappearance of spots, we found that new spots emerged by apparent simplification of an object: spot C appeared when the handle and hose were removed from the fire extinguisher. We have examined 12 pairs of activation patterns obtained before and after the simplification of the objects, and we observed changes in the distribution patterns consistent with either Fig. 12.4a or 12.4b for all of the pairs.

12.4 Visual features represented by individual spots

To directly address the neural mechanisms of appearance and disappearance of spots by object simplification, we recorded extracellular responses from 25 cells in the four spots shown in Fig. 12.4b, and analyzed the response properties of the cells in each spot. Figure 12.5 shows response properties of the representative cells in these spots. The difference in optical response patterns to stimuli *1* and *3* in Fig. 12.4b suggests that spots A and B represented visual features related to the handle and hose of the fire extinguisher. In fact, cells in spots A and B were significantly activated by the handle and hose in isolation (Fig. 12.5, a,*2* and b,*2*) as well as by the silhouette of the original fire extinguisher (Fig. 12.5, a,*1* and b,*1*). The cells in spot A were activated by the handle (Fig. 12.5, a,*3*) having protrusions, but not by the hose (Fig. 12.5, a,*4*). Furthermore, other stimuli with sharp protrusions, such as a 'hand' (Fig. 12.5, a,*5*) and cat's head (Fig. 12.5, a,*6*), also activated the cells. These cells seemed to require 'sharp protrusions' for activation. In contrast, cells in spot B were activated by the hose (Fig. 12.5, b,*4*) but neither by the handle (Fig. 12.5, b,*3*) nor a 'line segment' (Fig. 12.5, b,*5*). Thus we determined the critical feature as an 'asymmetric arc' (Fig. 12.5, b,*4*). The neural responses of cells in spots C and D were consistent with the imaging results in Fig. 12.4b: cells in spot C were activated by the 'cylinder' but not by the original fire

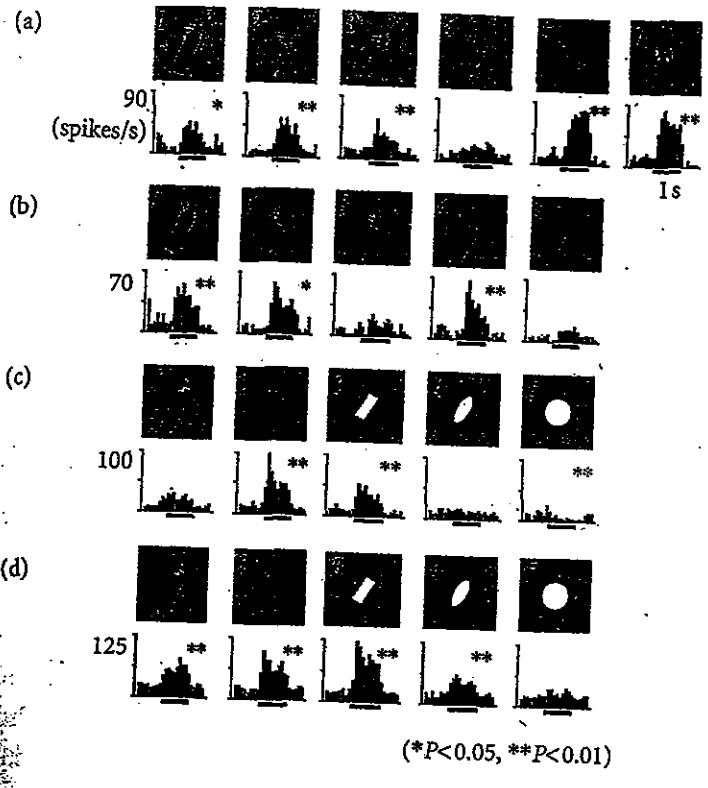

Fig. 12.5 Visual responsiveness of representative cells in spots A–D in Fig. 12.4b. (a), (b), (c), and (d) indicate responses in spots A (track 2, depth 620 μm), B (track 3, depth 540 μm), C (track 8, depth 280 μm), and D. (track 16, depth 280 μm), respectively. Red asterisks indicate significant inhibition ($P < 0.01$). (Adapted from Tsunoda *et al.* 2001.)

extinguisher (Fig. 12.5, c,*1* and c,*2*), and cells in spot D were significantly activated by both stimuli (Fig. 12.5, d,*1* and d,*2*). The critical feature for cells in spot D was a 'rectangular shape' (Fig. 12.5, d,*3*), but cells also responded significantly to an 'ellipse' (Fig. 12.5, d,*4*). Since there was no response to a 'circle' (Fig. 12.5, d,*5*), we determined the critical feature of the spots as an 'elongated structure'.

Similarly, the simplest visual feature that could activate the cells in spot C was a rectangular shape (Fig. 12.5, c,*3*). In contrast to the cells in spot D, however, there was no activation by an ellipse (Fig. 12.5, c,*4*). In addition, the cells were inhibited by a circle (Fig. 12.5, c,*5*). Thus, these results suggest that the response properties of the cells in spot C (Fig. 12.4b) are determined by the balance between excitatory and inhibitory inputs: the excitatory inputs were given by a feature related to a rectangular shape and the inhibitory inputs are given by a feature related to a circle. This explanation would account for the lack of activation by the fire extinguisher, where the hose (circular shape) attached to the rectangular cylinder makes the entire shape elliptical. These results suggest that some of the columns representing a particular feature are inactive when other features are presented together with that feature. This could explain the optical imaging results in which active spots appeared following simplification of the stimulus.

The extracellular recording shows that inhibitory mechanisms are involved in the responsiveness of the neurons in spot C (Fig. 12.5, c,*5*). Fujita and Fujita (1996) found

intrinsic excitatory connections that extend parallel to the cortical surface for long distances. The underlying anatomical substrate of the inhibitory mechanisms could be combination of the excitatory connections and local inhibitory circuits within a target column. Alternatively, inhibitory neurons may extend their axons directly to distant target columns, as in the case of basket cells in the cat primary visual cortex (Kisvarday *et al.* 1994). One other possibility is that inhibitory interactions within area TEO is reflected in area TE through columnar projections from area TEO to area TE (Saleem *et al.* 1993).

12.5 Object representation with a combination of active and inactive columns

The combination of intrinsic signal imaging and extracellular recording can suggest the spatial layout of neural activity evoked by complex objects. Intrinsic signal imaging showed distributed representation of object images in area TE: object images are represented as combinations of multiple spots (Fig. 12.3a). In general, there are two concepts of distributed representation, depending on the fraction of neurons in the population: sparsely distributed and densely distributed representation (Foldiak and Young 1995). Although Fig. 12.3a shows many active spots elicited by some of the stimuli, the region activated by a single object image was, on average, only 3.3 ± 2.5% of the entire recording area (number of examined object images = 37). This low density suggests a sparsely distributed representation of objects. Another finding was that object simplification resulted in systematic changes in the distribution patterns of spots. We found that 32 out of 106 activity spots (30%) disappeared when part of the visual features were removed from the stimuli by object simplification (Fig. 12.4a). Extracellular recording showed that the optimal stimuli for neurons in these spots were visual features less complex than the original objects. These results suggest that there are spots specific for the representation of a particular visual feature within an object image, and that an object image is represented by a combination of spots specified to these visual features (Fig. 12.6a, b). However, among 106 activity spots, 18 spots appeared only after stimulus simplification (Fig. 12.4b, spot C). These results cannot be explained by this scheme, which implicitly assumes that all the spots related to a single feature in an object image are activated (Fig. 12.6b). Thus, we propose an extended scheme of distributed representation, where objects are represented not by the simple sum of feature columns but by combinations of active and inactive spots for individual features (Fig. 12.6c). According to this scheme, we think that the fire extinguisher in Fig. 12.4b was represented not only by the active spots representing the handle (spot A), the hose (spot B), and the cylinder (spot D), but by the absence of spot C representing the entire elliptical structure. Combinations of inactive as well as active columns increase the number of available activation patterns, and thus, in general, could increase the number of objects to be specifically represented (Fig. 12.6c). From

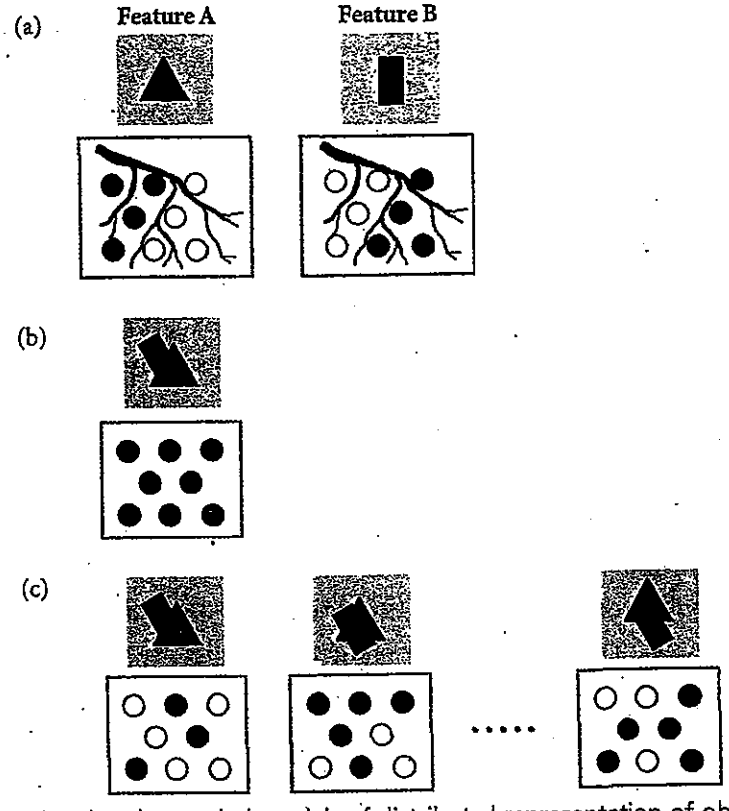

Fig. 12.6 Conventional and extended models of distributed representation of objects. Assuming that features A and B are represented by spots shown in red and blue, respectively, on the cortical surface (a), the visual stimulus consisting of these two features will activate all of these red and blue spots in models based on the conventional distributed representation (b). In our extended model, only a part of them are activated by the same stimulus (c). By this mechanism, stimuli consisting of the same features but arranged in different configurations can be represented by different activation patterns on the cortex. In each figure, the upper and lower panels indicate the visual stimulus and cortical area including spots responding to the stimulus.

physiological point of view, we consider the relationship between increased activation patterns and object representation in the following way:

In our scheme, we assume that a single visual feature maximally activates a set of columns (Fig. 12.6a). However, their tuning properties are not exactly the same, so that each column can represent additional information about visual images. For example, both spots C and D in Fig. 12.4b represent 'elongated structure'. But in addition, appearance of these spots depends on whether the given stimulus is elliptical or not. Then, objects differentiated by the additional information can be represented differently by activating a subset of these columns. One case would be representations of objects that consist of the same set of visual features but with a different arrangement of them. Another case would be representation of the same objects that look different under different vantage points, with partial occlusion, and with shading.

12.6 Representation of spatial arrangement of parts in object images

Examination of visual features represented by neurons in area TE suggested that at least some of the neurons in this area, represent 'local features' in object images, as neurons in spots A and B (Figs 12.4b and 12.5) represent 'protrusions' and 'asymmetric curvature', respectively. Since information about the spatial arrangement of 'local features' is necessary for the specific representation of object images, some of the other neurons may represent visual features related to the spatial arrangement of local features ('configurational information'). Here, we refer to 'local features' as visual features that occupy part of an object image and are distinguishable from other parts of an object image by their particular shapes, colors, or textures. 'Configurational information' is information about the spatial arrangement of "local features' themselves or about spatial arrangement of parts including local features. For example, intrinsic signal imaging with extracellular recording suggests that the presence or absence of activity in spot C constrains the spatial arrangement of the hose and the cylinder ('local features') of the fire extinguisher (Fig. 12.4b and Fig. 12.5c). This spot was activated when the hose is attached to the side of the cylinder and makes the entire shape elliptical, but may not be if the hose is secured above the handle where the rectangular shape of cylinder is exposed. Thus, we consider that activity in spot C has information about configuration to some extent, although this may be one way of representing a particular 'configurational information'.

To further examine the representation of 'configurational information', we investigated spots activated by an object (original, Fig. 12.7, 1) and the same object with a gap introduced between parts of the object (Fig. 12.7, 4), but not by a part alone (Fig. 12.7, 2 and 3) (Yamane *et al.* 2001). We suggest that these spots do not simply represent local features in objects, because either part is not essential for activation. Moreover, activation by the stimulus with an introduced gap indicates that local features appearing a

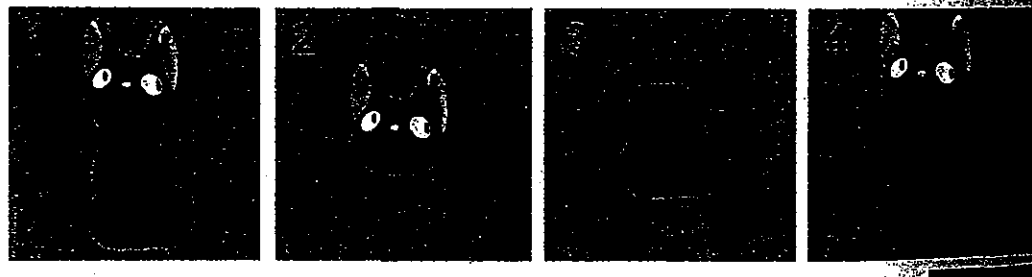

Fig. 12.7 A representative set of visual stimuli used in intrinsic signal imaging for examination of the representation of the spatial arrangement of parts. The response properties shown in Figs. 12.8 and 12.9 were obtained from a spot activated by stimuli 1 and 4, but not by stimuli 2 and 3.

the junction of two parts, such as sharp connecting corners in Fig. 12.7, stimulus 1, are also not essential. We recorded single-cell responses from a spot having stimulus selectivity described above, and found three characteristic response properties ($n = 14$):

(1) These cells had critical features which were combinations of two vertically aligned parts (Fig. 12.8a, see also Fig. 12.1). There was no activation by either part (Fig. 12.1, step 4).

(2) These cells were less sensitive to color, texture, and local shapes of either part. Three findings suggest this conclusion. First, there were no changes in the responses after removing color and texture during the stimulus simplification procedure (Fig. 12.1 and 12.8a). Secondly, changes in the shapes of the parts did not alter responses of these neurons very much. For example, a neuron, whose critical feature was determined as a combination of a circle and a rectangle, was also significantly activated by a combination of a circle and an ellipse (data not shown). Finally, these cells responded equally well to object images even having different color, texture, and local shapes, as long as they had the global shape similar to the critical features (Figs 12.8b and 12.9).

(3) These cells were highly selective to a particular position of the upper part relative to the lower part (Fig. 12.10).

These characteristic response properties enable these neurons to respond to visual stimuli regardless of the local features embedded in either part, but only when these local features are aligned in particular orientation, as in Fig. 12.10. These results, as well

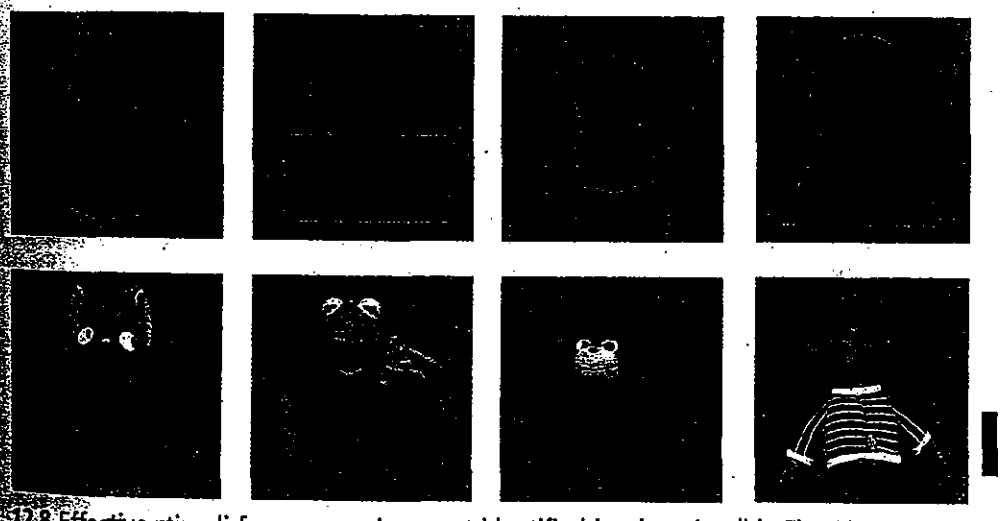

Fig. 12.8 Effective stimuli for neurons in a spot identified by the stimuli in Fig. 12.7. (a) Representative critical features determined by stimulus simplification. Please note that, when color and texture are not essential, the stimulus was filled black (see Fig. 12.1). (b) The best object stimuli for these neurons, among 100 object stimuli examined before stimulus simplification. Scale bar, 5°.

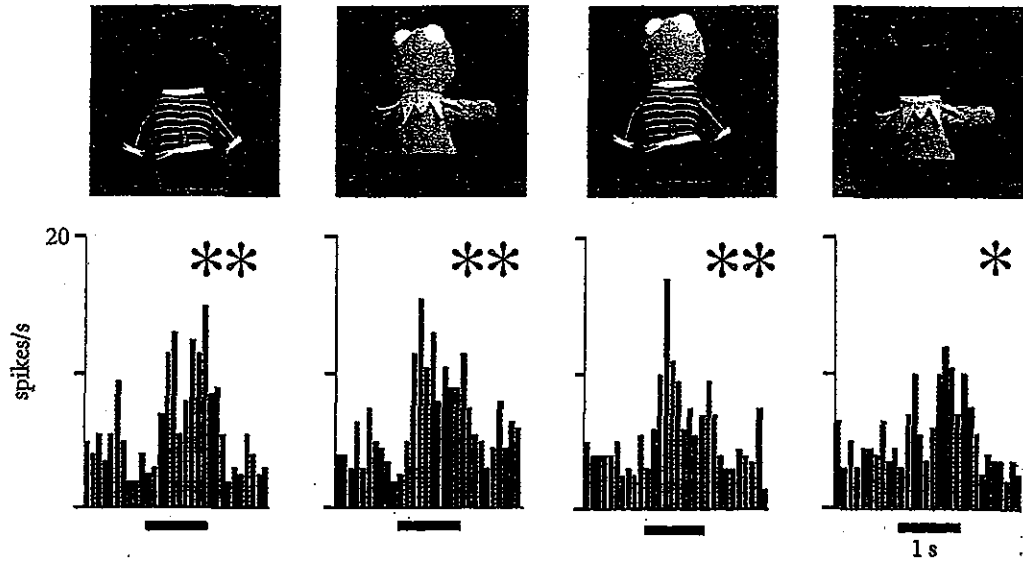

Fig. 12.9 Neural responses of one representative neuron to object stimuli. Upper panel shows visual stimuli, and lower panel indicates peristimulus–time histograms (PSTHs) showing responses of the neuron to the stimuli given above. The stimulus was presented for a period of 1 s, indicated by the horizontal line segment in each PSTH. These stimuli activated the cell equally well. $*P < 0.05$, $**P < 0.01$.

as neurons in spot C in Fig. 12.4b, suggest that neurons in area TE do not necessarily represent local features but also configurational information of the object image. Object images could be specifically represented by a combination of spots representing 'local features' and those representing 'configurational information'.

12.7 Face-specific neurons in area TE

'Face neurons' are representative neurons in area TE responding to the visual images of familiar objects. We consider that 'face neurons' also represent 'configurational information'. 'Face neurons' respond to 'faces', but these responses cannot be explained by specific responses to a part of the 'face' (Fig. 12.11). In this particular case, for example, a face without eyes did not activate the cell, but there was no activation by 'eyes' alone (Fig. 12.11b, c). Furthermore, previous studies have shown that a 'face' with scrambled facial parts does not activate these neurons (Desimone *et al.* 1984). There are two characteristic properties of 'face neurons'. First, many of them are broadly tuned to images of faces from a particular vantage point (Fig. 12.11a; Desimone *et al.* 1984; Perrett *et al.* 1991). Secondly, these cells have sensitivity to individual faces, but the tunings are broad (Perrett *et al.* 1984; Baylis *et al.* 1985; Yamane *et al.* 1988; Young and Yamane 1992). These response properties suggest that face neurons represent the 'configuration' specific to faces.

Intrinsic signal imaging showed that there are spots specifically activated by faces (Wang *et al.* 1996, 1998) (Fig. 12.12). Thus, face neurons, as well as neurons specific to

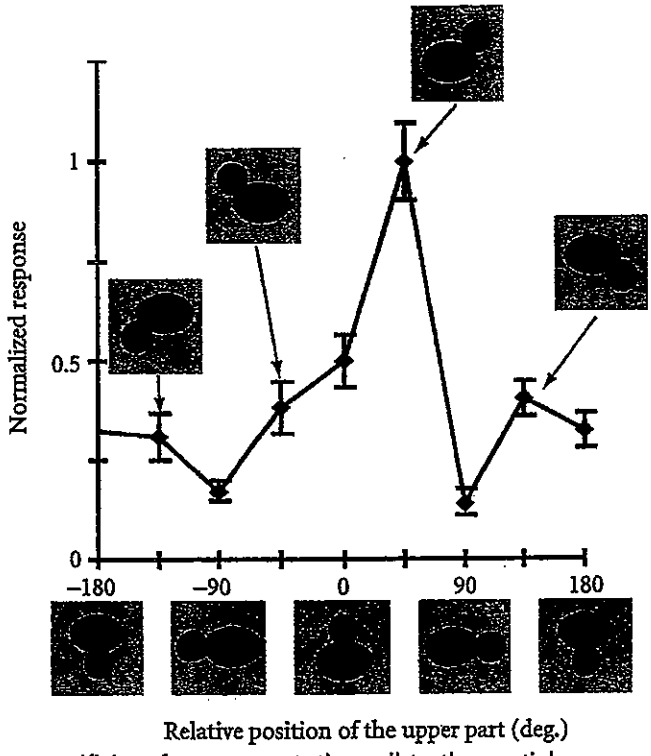

Fig. 12.10 Response specificity of a representative cell to the spatial arrangement of parts. The upper part of the critical feature of the cell was rotated relative to the lower part. The horizontal axis indicates the angle between the line connecting the center of upper and lower parts of each stimulus and that of the critical feature. The vertical axis indicates normalized value of stimulus evoked responses. In this particular case, the best response was elicited by the stimulus with 45°, but this is not only the case. Some other neurons respond maximally at 0°. It may be the case that neurons with different angles are located in close vicinity, as is the case for face columns (Fig. 12.12).

responding to visual features, are clustered together. Furthermore, activation patterns produced by images of faces from different vantage points revealed that the peaks of activity spots shift along the cortical surface as the face rotates from the left profile, to the right profile, through the front face. This representation of faces from different vantage points in close vicinity may be important for view-independent recognition of faces.

12.8 Summary and conclusions

In summary, our results from both optical and extracellular recordings provide evidence that a complex object is represented by combinations of columns in area TE, each of which represents visual features of the object image. The combinations are not simply based on summing up of the columns, but may instead rely on a combination of active and inactive columns to represent objects. These columns do not necessarily

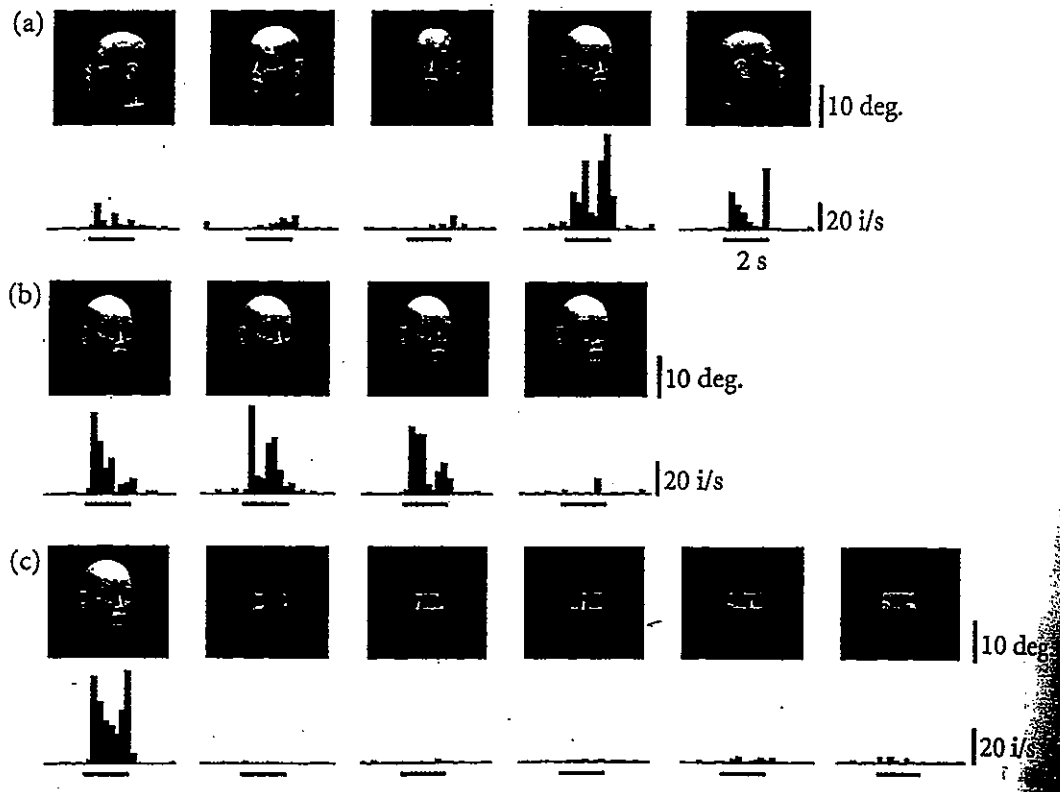

Fig. 12.11 Response properties of a typical face neuron shown by the PSTHs of neural responses evoked by stimuli given above. The recording consisted of three sessions. In the first session, (a), we examined selectivity of the neuron to a face at different vantage points. In the second session, (b), we examined the same neuron with face stimuli lacking different parts of the face. In the final session, (c), we examined responses to insolated eyes from different vantage points.

represent 'local features' but some of them may represent visual features related to 'configurational information'. We consider that neurons specific for images of familiar objects, such as 'faces', also represent visual features specific for these objects. For example, face neurons may represent 'configuration' specific for 'faces'. An image of a particular face could be represented by a combination of columns. Some of these columns represent 'local feature' specific to an individual, and others represent configurational information about the face at a particular vantage point.

Visual features represented in area TE seem to range from simple features such as 'rectangular shape' to highly complex visual features such as 'configuration of ...'. Although there is no direct evidence, this wide range of complexity in visual features may be produced through experience-dependent association of visual features. For example, neurons responding to vertically aligned parts (Fig. 12.8) may be generated because monkeys frequently experience objects having such a part arrangement. In support, in monkeys trained with a particular set of visual stimuli, previous studies revealed that some neurons specifically responded to visual stimuli that became ...

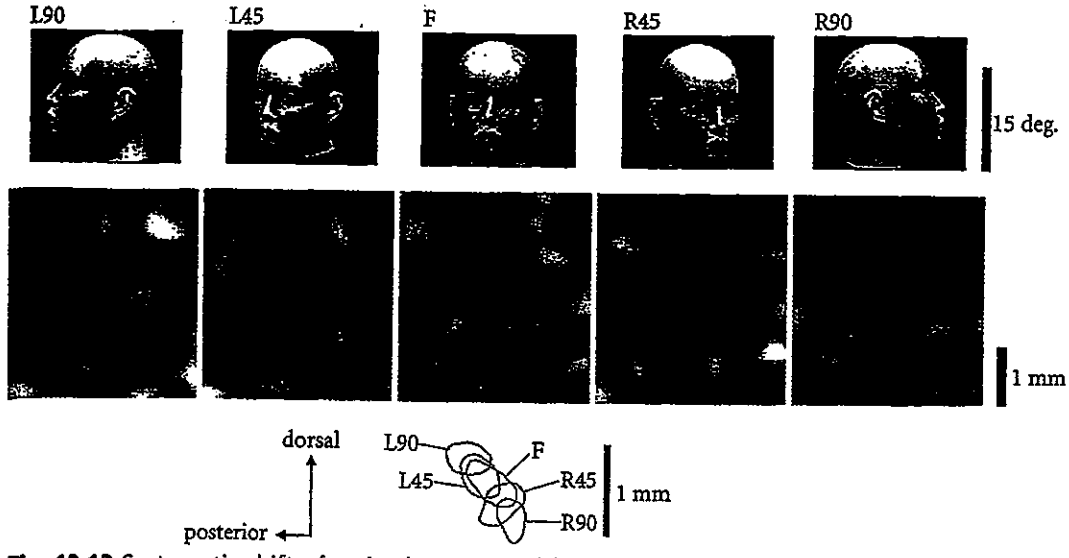

Fig. 12.12 Systematic shift of activation spots with rotation of the face. Images of the same cortical area (middle panels) obtained for five different views of the same mannequin face (top panels). The contours of the activity spots are superimposed at the bottom. (Adapted from Wang *et al.* 1996 Permission sought.)

through training (Logothetis *et al.* 1995; Kobatake *et al.* 1998). Those visual stimuli could represent 'local features' or 'configurational information' depending on the stimulus set and the task design.

Acknowledgements

We thank R. Uma Maheswari, Kathleen Rockland, and Charles Rockland for helpful comments on the manuscript. This work was partly supported by Research Fellowships of the Japan Society for the Promotion of Young Scientists to Y.Y.

References

Davis, G.C., Rolls, E.T., and Leonard, C.M. (1985) Selectivity between faces in the responses of a population of neurons in the cortex in the superior temporal sulcus of the monkey. *Brain Res.* 342, 91–102.

Desimone, R., Albright, T.D., Gross, C.G., and Bruce, C. (1984) Stimulus-selective properties of inferior temporal neurons in the macaque. *J. Neurosci.* 4, 2051–62.

Field, P. and Young, M.P. (1995) Sparse coding in the primate cortex. In M.A. Arbib (ed.) *The handbook of brain theory and neural networks* (pp. 895–8). MIT Press, Cambridge MA.

Fujita, I. and Fujita, T. (1996) Intrinsic connections in the macaque inferior temporal cortex. *J. Comp. Neurol.* 368, 467–86.

Fujita, I., Tanaka, K., Ito, M., and Cheng, K. (1992) Columns for visual features of objects in monkey inferotemporal cortex. *Nature* 360, 343–6.

Gochin, P.M., Miller, E.K., Gross, C.G., and Gerstein, G.L. (1991) Functional interactions among neurons in inferior temporal cortex of the awake macaque. *Exp. Brain Res.* 84, 505–16.

Grinvald, A., Shoham, D., Shmuel, A., Glaser, D., Vanzetta, I., Shtoyerman, E., Slovin, H., Wijnbergen, C., Hildesheim, R., and Arieli, A. (1999) In-vivo optical imaging of cortical architecture and dynamics. In U. Windhorst and H. Johansson (Eds.), *Modern techniques in neuroscience research* (pp. 893–970). Springer, Berlin.

Gross, C.G., Rocha-Miranda, C.E., and Bender, D.B. (1972) Visual properties of neurons in inferotemporal cortex of the Macaque. *J. Neurophysiol.* 35, 96–111.

Kisvarday, Z.F., Kim, D-S., Eysel, U.T., and Bonhoeffer, T. (1994) Relationship between lateral inhibitory connections and the topography of the orientation map in cat visual cortex. *Eur. J. Neurosci.* 6, 1619–32.

Kobatake, E. and Tanaka, K. (1994) Neuronal selectivities to complex object features in the ventral visual pathway of the macaque cerebral cortex. *J. Neurophysiol.* 71, 856–67.

Kobatake, E., Wang, G., and Tanaka, K. (1998) Effects of shape-discrimination training on the selectivity of inferotemporal cells in adult monkeys. *J. Neurophysiol.* 80, 324–30.

Logothetis, N.K., Pauls, J., and Poggio, T. (1995) Shape representation in the inferior temporal cortex of monkeys. *Curr. Biol.* 5, 552–63.

Malach, R., Reppas, J.B., Benson, R.R., Kwong, K.K., Jiang, H., Kennedy, W.A., Ledden, P.J., Brady, T.J., Rosen, B.R., and Tootell, R.B. (1995) Object-related activity revealed by functional magnetic resonance imaging in human occipital cortex. *Proc. Natl Acad. Sci. USA* 92, 8135–39.

Perrett, D.I., Rolls, E.T., and Caan, W. (1982) Visual neurones responsive to faces in the monkey temporal cortex. *Exp. Brain Res.* 47, 329–42.

Perrett, D.I., Smith, P.A.J., Potter, D.D., Mistlin, A.J., Head, A.S., Milner, A.D., and Jeeves, M.A. (1984) Neurons responsive to faces in the temporal cortex: studies of functional organization, sensitivity to identity and relation to perception. *Hum. Neurobiol.* 3, 197–208.

Perrett, D.I., Oram, M.W., Harries, M.H., Bevan, R., Hietanen, J.K., Benson, P.J., and Thomas, S. (1991) Viewer-centered and object-centered coding of heads in the macaque temporal cortex. *Exp. Brain. Res.* 86, 159–73.

Saleem, K.S., Tanaka, K., and Rockland, K.S. (1993) Specific and columnar projection from area TEO to TE in the macaque inferotemporal cortex. *Cerebr. Cortex* 3, 454–64.

Tanaka, K., Saito, H., Fukada, Y., and Moriya, M. (1991) Coding visual images of objects in the inferotemporal cortex of the macaque monkey. *J. Neurophysiol.* 66, 170–89.

Tsunoda, K., Yamane, Y., Nishizaki, M., and Tanifuji, M. (2001) Complex objects are represented in macaque inferotemporal cortex by the combination of feature columns. *Nat. Neurosci.* 4, 832–8.

Wang, G., Tanaka, K., and Tanifuji, M. (1996) Optical imaging of functional organization in the monkey inferotemporal cortex. *Science* 272, 1665–8.

Wang, G., Tanifuji, M., and Tanaka, K. (1998) Functional architecture in monkey inferotemporal cortex revealed by in vivo optical imaging. *Neurosci. Res.* 32, 33–46.

Yamane, S., Kaji, S., and Kawano, K. (1988) What facial features activate face neurons in the inferotemporal cortex of the monkey? *Exp. Brain. Res.* 73, 209–14.

Yamane, Y., Tsunoda, K., Matsumoto, M., Phillips, A., and Tanifuji, M. (2001) Decomposition of object images by feature columns in macaque inferotemporal cortex. *Neurosci. abstr* 399.6.

Young, M.P. and Yamane, S. (1992) Sparse population coding of faces in the inferotemporal cortex. *Science* 256, 1327–31.

Cerebral Cortex Advance Access published September 30, 2004

Localization of Activity-dependent Changes in Blood Volume to Submillimeter-scale Functional Domains in Cat Visual Cortex

Mitsuhiro Fukuda[1,2], Uma Maheswari Rajagopalan[1], Ryota Homma[1], Madoka Matsumoto[1,3], Makoto Nishizaki[1,4] and Manabu Tanifuji[1]

[1]Laboratory for Integrative Neural Systems, RIKEN Brain Science Institute, 2-1 Hirosawa, Wako-shi, Saitama, 351-0198, Japan
[2]Present address: Department of Neurobiology, Brain Imaging Research Center, University of Pittsburgh, 3025 East Carson Street, PA 15203, USA
[3]Present address: Laboratory for Cognitive Brain Mapping, RIKEN Brain Science Institute, 2-1 Hirosawa, Wako-shi, Saitama, 351-0198, Japan
[4]Present address: Advanced Technology Research Laboratories, Matsushita Electric Industrial Co., Ltd., 3-10-1 Higashimita, Tama-ku, Kawasaki-shi, 214-8501, Japan

We have examined whether blood volume changes induced by neural activation are controlled precisely enough for us to visualize the submillimeter-scale functional structure in anesthetized and awake cat visual cortex. To activate the submillimeter-scale functional structures such as iso-orientation domains in the cortex, visual stimuli (gratings) were presented to the cats. Two methods were used to examine the spatial precision of blood volume changes including changes in total hemoglobin content and changes in plasma volume: (i) intrinsic signal imaging at the wavelength of hemoglobin's isosbestic point (569 nm) and (ii) imaging of absorption changes of an intravenously injected dye. Both measurements showed that the visual stimuli elicited stimulus-nonspecific and stimulus-specific blood volume changes in the cortex. The former was not spatially localized, while the latter was confined to iso-orientation domains. From the measurement of spatial separation of the iso-orientation domains, we estimated the spatial resolution of stimulus-specific blood volume changes to be as high as 0.6 mm. The changes in stimulus-nonspecific and -specific blood volume were not linearly correlated. These results suggest the existence of fine blood volume control mechanisms in the capillary bed in addition to global control mechanisms in arteries.

Keywords: cerebral blood flow, functional MRI, hemodynamic response, intrinsic signal imaging, orientation column, spectroscopic analysis

Introduction

The activation of cortical neurons elicits changes in light reflection from an exposed cortical surface. The measurement of these light reflection changes (intrinsic signals) enables cortical functional structures to be visualized at submillimeter-scale spatial resolution and provides profound insights into cortical functions in visual areas (Grinvald *et al.*, 1986; Ts'o *et al.*, 1990; Bonhoeffer and Grinvald, 1991, 1993; Malonek *et al.*, 1994; Roe and Ts'o, 1995; Wang *et al.*, 1996, 1998; Ghose and Ts'o, 1997; Tsunoda *et al.*, 2001).

Circumstantial evidence suggests that hemodynamic responses, such as changes in deoxyhemoglobin (Hbr) concentration and blood volume changes, are the major sources of intrinsic signals at visible wavelengths (Frostig *et al.*, 1990; Bonhoeffer and Grinvald, 1996; Malonek and Grinvald 1996). Decreases in light reflection (i.e. increases in light absorption) at 600–630 nm, where the absorption coefficient of Hbr is 5–10 times higher than that of oxyhemoglobin (HbO_2) (Fig. 1 inset), suggest that increases in Hbr concentration are accompanied by the oxygen consumption of activated neurons (Silver, 1978; Sibson *et al.*, 1998; Thompson *et al.*, 2003). The decrease in light reflection at the wavelength where the absorption coefficient of HbO_2 equals that of Hbr (i.e. hemoglobin's isosbestic point) suggests that an increase in total hemoglobin (Hbt) concentration (blood volume change) is another component of the signal. In addition to these hemodynamic components, activity-dependent light scattering (Ls) changes (MacVicar and Hochman, 1991; Holthoff and Witte, 1996) may also be involved in intrinsic signals at wavelengths >700 nm, at which the absorption coefficients of both HbO_2 and Hbr are relatively small (Maheswari *et al.*, 2003).

Since hemodynamic responses are the basis of modern functional brain imaging techniques such as positron emission tomography (PET) and functional magnetic resonance imaging (fMRI), it is very important to characterize their spatial and temporal properties. Analyses of intrinsic signals at visible wavelengths provide clues that can lead to an understanding of these properties. Malonek and Grinvald (1996) applied spectroscopy to the analysis of intrinsic signals in the cat visual cortex, and found that increases in Hbr concentration were confined to iso-orientation domains, but increases in HbO_2 concentrations were less localized. These results suggest that blood inflow to an activated area is not strongly confined to submillimeter-scale functional domains. However, Duong *et al.* (2001) have recently demonstrated using cerebral-blood-flow (CBF)-based fMRI that blood flow changes are strongly localized to iso-orientation domains in the cat visual cortex. Similarly, an earlier work suggested that blood volume changes associated with changes in blood inflow are localized in active domains (Frostig *et al.* 1990). Thus, the spatial specificities of blood flow changes and associated blood volume changes are still unresolved. In particular, because of the lack of detailed examinations, the specificity of blood volume changes remains unconfirmed. Here, we characterized spatial and temporal patterns of blood volume changes in the cat visual cortex using two methods: (i) intrinsic signal imaging at the wavelength of hemoglobin's isosbestic point, and (ii) imaging of absorption changes of an intravenously injected absorption dye.

Materials and Methods

Eighteen cats (2–6 months of age, 1.0–3.3 kg) were used under anesthesia; five of the animals were also used in the awake state. All procedures were conducted following the 'Guiding Principles for the Care and Use of Animals in the Field of Physiological Sciences' (The

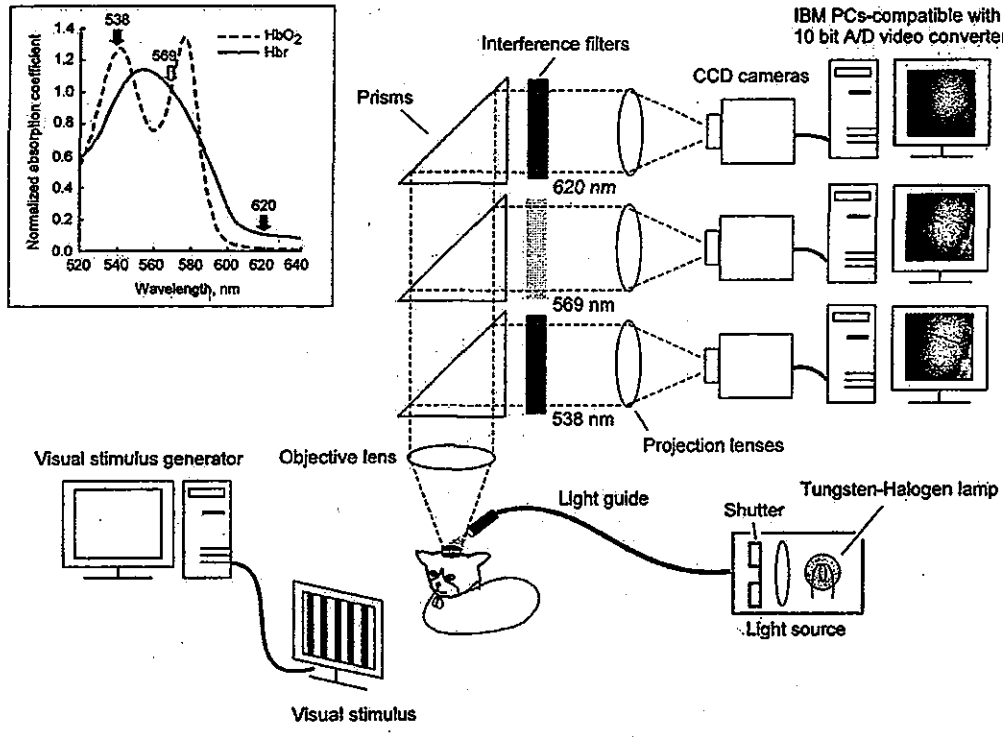

Figure 1. Scheme of the multiple wavelength imaging system. The cortical surface is illuminated with white light. Reflected light is collected by an objective lens and divided into three light paths by prisms. Each beam passes through an interference filter and is focused onto the target plane of the video cameras by projection lenses. The inset on the upper left corner shows absorption spectra of HbO_2 and Hbr. The arrows indicate central wavelengths of the three filters we used (538, 569 and 620 nm). The absorption coefficients of HbO_2 and Hbr at different wavelengths were obtained from *in vitro* experiments and normalized to the absorption coefficient at 569 nm. The normalized coefficients of HbO_2 and Hbr at 538 nm were 1.23 and 0.91 respectively. Similarly, at 620 nm the normalized coefficients of HbO_2 and Hbr were 0.01 and 0.11 respectively.

Physiological Society of Japan), and with the approval of the RIKEN Committee on Animal Research.

Animal Preparations

Cats were initially anesthetized with an inhalation of isoflurane (2-2.5%) in a mixture of 50% N_2O and 50% O_2. After tracheal cannulation, anesthesia was maintained with a mixture of 70% N_2O and 30% O_2 supplemented with 1-2% isoflurane. The cephalic vein was catheterized and neuromuscular blockade was carried out by continuous infusion of pancuronium bromide (0.2 mg/kg/h) mixed with dexamethazone (0.05 mg/kg/h) and 7.5% glucose in lactose-containing Ringer's solution. The cats were then artificially ventilated. To prevent the cornea from drying, contact lenses were fitted to the eyes. We continuously monitored rectal temperature, electroencephalogram (EEG), electrocardiogram (ECG), and expired CO_2 to assess the depth of anesthesia. Rectal temperature was maintained at 37.5-38.5 °C with a feedback-regulated heating pad system. The expired CO_2 was maintained between 3.0 and 4.0%.

On the first day of recording, a cat was placed in a stereotaxic apparatus (SN-3N, Narishige). Under aseptic surgery, we first attached with dental acrylic cement a metal post to fix its head and a stainless steel chamber (18 mm inner diameter, Nakazawa-Seisaku, Japan) for optical imaging to the skull. The metal post was placed approximately above the bregma. The chamber was placed such that it included area 17 or the border between areas 17 and 18 (in Horsley-Clarke coordinates, approximately A5-P10 for area 17 and A10-P5 for the border between areas 17 and 18). We then performed craniotomy inside the chamber, and resected the dura mater. The inside of the chamber was then filled with 1.5-2.0% agarose (Agarose-HGS, gel strength 1.5%; Nacalai Tesque, Japan) containing dexamethazone (0.1 mg) and an antibiotic (gentamicin, 0.25 mg). Finally, the chamber was covered with a round glass coverslip and sealed with a screw-top lid including a silicone gasket. We could observe the cortical surface clearly through the glass coverslip and could visualize the same functional structures repeatedly for 2-3 weeks without cleaning the inside of the chamber. After the surgery and the recordings, an appropriate antibiotic (cefodizime sodium, 60 mg/kg i.m.) was administered to the cat before returning the animal to its home cage.

During recordings on the first and subsequent days, the cat's head was immobilized with a head post instead of ear bars. Pupils were dilated by applying 0.5% tropicamide and 0.5% phenylephrine hydrochloride. The isoflurane concentration was maintained at 0.5-1.0% during the recordings. The other conditions were the same as those in the initial surgery described above.

Visual Stimuli

Square wave gratings (white: 8 cd/m^2; black: 0 cd/m^2) were generated with a VSG2/3 graphics video board (Cambridge Research Systems, Rochester, UK), controlled by homemade software, and were presented on a monitor screen (640 × 480 pixels and 100 Hz refresh rate, GDM-20SE3T, Sony). The spatial frequency and the drifting velocity of the gratings were 0.5 cycles/deg and 4 deg/s for area 17, and 0.15 cycles/deg and 15 deg/s for area 18 (Bonhoeffer *et al.*, 1995). The drifting direction was reversed every 0.5 s during a 2 s stimulus presentation. Two or four stimuli [orientations, 0° (horizontal), 45°, 90° and 135°] together with a blank screen (homogenous gray, 4 cd/m^2) as a control were presented in a pseudorandom order. In the experiment using awake cats, we used stationary grating patterns flickering at 5 Hz (8 Hz in one cat) to minimize the effect of eye movements following the grating motion. The same flickering gratings were also used in the examination of the same cats under anesthesia for comparison.

The center of a cat's visual field was estimated by projecting images of optic disks and patterns of surrounding vessels onto the monitor screen in front of the cat. The screen was placed at a distance ranging from 20 to 40 cm, where the best focus of the optic disks and the patterns of surrounding vessels were obtained for each cat. At these distances the size of the screen corresponded to 43°-86° (width) × 36°-71° (height)

of the cat's visual field. In the experiment with awake cats, the screen was placed 20 cm in front of the animals.

Optical Imaging of Intrinsic Signals

We developed a multiple wavelength imaging system equipped with three identical cameras (Sanso-Seisaku, Japan) that enabled us to simultaneously record intrinsic signals at three different wavelengths (Fig. 1). We used two sets with the same configuration: one was equipped with CID-2221D video cameras (CIDTEC, Liverpool, NY), and the other was equipped with CS8310 video cameras (Tokyo Electric Industry, Japan). The exposed cortical surface was illuminated with white light using eight fiber optic bundles placed around the chamber, which were connected to two tungsten-halogen bulbs (82 V, 300 W; Philips) driven by stabilized DC power supplies (PD110-5D; Kenwood, Japan). The duration of exposure of the cortical surface to the light was restricted to 10 s using a mechanical shutter, which opened 2 s before starting image acquisition. Reflected light from the cortical surface was collected by an objective lens, and divided into three separate paths by prisms. Each light beam passed through an interference filter tuned to one of three different wavelengths (538, 569 and 620 ± 10 nm; Asahi Spectra, Japan) and focused onto one of three video cameras by each projection lens. A combination of objective and projection lenses constituted the tandem-lens optics (Ratzlaff and Grinvald, 1991). Using different combinations of a projection lens (50 mm, f1.2; Nikon, Japan) and an objective lens (35 mm, f1.4 or 50 mm, f1.2; Nikon, Japan), imaging areas were 4.9 × 4.9 mm^2 or 7.0 × 7.0 mm^2 for the CID-2221D camera (256 × 256 pixels) and 8.8 × 6.6 mm^2 for the CS8310 camera (640 × 480 pixels). The imaging areas of the three cameras were adjusted to overlap in order to record signals from the same region of the cortical surface. Video signals from the three cameras were separately digitized with 10-bit video A/D converter boards (Pulsar, Matrox Graphics Inc., Canada) on three computers. These computers synchronously acquired 240 frames at a frame rate of 1/30 s for the CS8310 camera or 1/60 s for the CID-2221D camera. Fifteen consecutive frames for the CS8310 camera or 15 alternate frames for the CID-2221D camera were averaged on-line. Consequently, 16 images were acquired with a temporal resolution of 500 ms (i.e. 8 s). Acquired images were stored on hard disks without binning for the CID-2221D camera (256 × 256 pixels) and with binning (2 × 2 pixels were combined into a single pixel) for the CS8310 camera (i.e. 320 × 240 pixels).

Images of the cortical surface were taken using these cameras and the focal plane was changed from the cortical surface to 700–800 μm below. The maximum intensities of video signals from the three cameras were adjusted to near-saturation level by changing the intensity of incident light and camera gains. The black levels of each video signal (a video signal obtained under complete darkness, ~10% of saturation level) were then recorded for off-line data processing. In the experiment with anesthetized cats, data acquisition was started at a certain phase of respiration in synchrony with heartbeat. A visual stimulus appeared 1 s after the onset of image acquisition. To allow the relaxation of vascular responses to the previous stimulation, the interstimulus interval (ISI) was set at 30 s. Data of four trials using the same stimulus were averaged online and saved as one block. We recorded 20 blocks in one experiment; altogether, responses for 80 trials (20 blocks, 4 trials per block) were acquired for each stimulus.

In the recordings with awake cats, the body of the cat was placed into a loosely fitting pouch and the head was immobilized by the implanted head post. The cats quickly became accustomed to the restriction of movements and presented no signs of discomfort during the experiments. To minimize visual input from surroundings, the experiments were performed in a dark room and mechanical shutters were placed in front of the cat's eyes. The shutters were only opened during the stimulus presentation. Unlike the experiment under anesthesia, data acquisition was not synchronized with respiration and heartbeat. The total recording period was restricted to 1.5 h/day to maintain the cats' alertness level. Data from 40 trials were averaged (20 blocks, 2 trials per a block) for each stimulus in one day. The experiments were repeated for two successive days and the data from the two days were finally averaged. The temporal and spatial patterns of intrinsic signals on the first day were almost identical to those on the second day (data not shown). The data from the same cat under anesthesia were also collected. To ensure that recordings were taken from the same region, we did not change the camera position relative to the head post until a series of experiments for the cat had been completed. We did not observe a misalignment of cortical vascular patterns in the series of experiments.

Imaging of Changes in Blood Volume with Intravascular Absorption Dye

For the measurement of changes in blood volume, we injected a light-absorbing dye (Nigrosin, water-soluble Acid Black 2; Sigma) through the cat's cephalic vein and recorded the stimulus-evoked absorption changes at 620 nm. We chose absorption dye instead of fluorescent dyes, which have previously been used for the measurement of blood volume (Frostig *et al.*, 1990; Narayan *et al.*, 1995; Cannestra *et al.*, 1998), because (i) fluorescent dye signals are in general too weak to resolve small changes such as stimulus-specific components, (ii) there is minimal effect of dye bleaching, and (iii) the same optics can be employed to assess the dye-specific responses immediately after the intrinsic signal imaging. The dye was dissolved in saline, filtered using a Millipore filter (0.22 μm pore size, Millipore Co. Bedford, MA), and injected prior to recording (final dosage, 20–34 mg/kg nigrosin for five cats). The physiological conditions (e.g. heart rate) of the cats did not change following the injection of the dye. Since the dye absorbed the incident light, the reflected light intensity from the cortical surface decreased after the dye injection. The intensity of the reflected light was readjusted to the saturation level of video signals prior to recording by increasing the incident light intensity. Data from 20–80 trials were averaged (5 to 20 blocks, 4 trials per block) for each stimulus.

Data Analysis

We analyzed all images pixel by pixel using IDL 5.4 (Research Systems, Inc.). The statistical significance of the data was evaluated by *t*-test (two-tailed, paired). The first step in the data analysis was to extract reflected light intensity from video signals by subtracting the image obtained in complete darkness (the black level) from the 16 consecutive images (8 s at 0.5 s/image). A change in reflected light intensity (intrinsic signals) was then expressed as the change in the optical density (ΔOD) as follows:

$$\Delta OD(t)_\lambda = \ln\{I_\lambda^{pre}/I_\lambda(t)\} \quad (1)$$

where I_λ^{pre} is the average of reflected light intensity before stimulus onset (1 s) at a wavelength λ, and $I_\lambda(t)$ is the reflected light intensity at t s from the stimulus onset. We calculated ΔODs for the individual stimuli and for the control (blank screen), and then subtracted ΔOD for the control from ΔOD for the grating stimuli to remove artifacts due to the respiratory cycle.

To demonstrate the spatial patterns of iso-orientation domains, differential images were generated by subtracting responses to one orientation from those to the orthogonal orientation. The differential images were then temporally averaged from 1 to 7 s after stimulus onset and processed using a Gaussian spatial filter (cutoff frequencies, σ = 10/mm for a high cutoff frequency and 1/mm for a low cutoff frequency for images obtained by the CS8310 camera, and σ = 5/mm for high cut-off and 1/mm for low cutoff for images obtained by the CID-2221D camera). The similarity between two differential images obtained at different wavelengths was quantified by calculating a correlation coefficient on pixel-by-pixel basis. In particular, when two pairs of orthogonal stimuli (the combination of 0° and 90° or that of 45° and 135°) were used at these wavelengths, a correlation coefficient of differential images was calculated for each pair separately, and then an average of the correlation coefficients was used to evaluate the similarity of differential images obtained at these wavelengths.

To quantitatively examine the intensities of intrinsic signals we averaged pixels in the region of interest (ROI). Pixels covering surface vessels thicker than 50 μm and those located outside of the cortex were excluded from the ROI. We divided ROI into active and less-active domains and averaged pixels of the active domains separately from pixels of the less-active domains. The active and less-active domains were determined on the basis of a differential image at 620 nm processed with the spatial filter. Pixels having positive values in the

differential image were assigned to the active domains and the remaining pixels were assigned to the less-active domains. The difference in the signal intensity between two domains was calculated by subtracting the average pixel value for the less-active domains from that for the active domains.

To quantify the spatial resolution of intrinsic signals, we measured the distance between neighboring iso-orientation domains in differential images. The distance between neighboring iso-orientation domains in the differential image was evaluated using an auto-correlation map of the differential image using NIH Image software (Scion Corporation) since the pattern of iso-orientation domains seems to have a periodic structure. The differential image used for this analysis was not processed by any spatial filter. The autocorrelation map was calculated for an ROI of 128 × 128 pixels (2.5 × 2.5 mm^2 for the CID-2221D camera with a 35 mm objective lens and 3.5 × 3.5 mm^2 for the CID-2221D and CS8310 cameras with a 50 mm objective lens) in the differential images. We then extracted the profile of the autocorrelation map along the central and secondary largest peaks. We assigned the distance between these two peaks as the distance between neighboring iso-orientation domains assuming that the periodic structure of the iso-orientation domains is the most dominant one in the map. The size of iso-orientation domains was estimated by measuring full width at half-maximum (FWHM) of the center peak of the profile.

Results

Definition of Stimulus-specific and Stimulus-nonspecific Components of Intrinsic Signals

Figure 2*A,B* shows the spatiotemporal patterns of the intrinsic signal at 620 nm in cat visual cortex induced by full-field grating stimuli. The grating stimuli evoked initial increases in light absorption (darkening of the cortex), which were followed by absorption decreases across the baseline (lightening of the cortex). These absorption changes were not spatially confined to domains specific for particular stimulus orientations. As reported previously (Grinvald *et al.*, 1986), two orthogonal orientations elicited a common absorption increase over the entire range (stimulus-nonspecific component), which was locally modulated in a stimulus-specific manner (stimulus-specific component) (Fig. 2*D*). Since this stimulus-specific modulation is complementary in two orthogonal orientations (Fig. 2*D*, red and blue lines), the region showing this stimulus specificity was extracted by subtracting the response for one orientation from that for the orthogonal orientation (Fig. 2*C*, and Fig. 2*D*, green line). We define regions where a stimulus elicited a larger absorption than the orthogonal stimulus, such as the shaded regions shown in Figure 2*D*, as 'active domains' for the stimulus. On the other hand, we define regions where the stimulus elicited smaller increases in absorption than the orthogonal stimulus as 'less-active domains' for the stimulus. For the analysis of the stimulus-nonspecific component, we averaged the intrinsic signals regardless of whether the domain was active or less active. For the analysis of the stimulus-specific component, we subtracted the intrinsic signal for the less-active domains from the signal for the active domains (see also Materials and Methods).

Time Courses of Stimulus-nonspecific and Stimulus-specific Components of Intrinsic Signals

As an approximation, we assume that Hbr and HbO_2 concentration changes are the major sources of intrinsic signals at visible wavelengths. Intrinsic signals at 620 and 569 nm then correspond approximately to changes in Hbr concentration and that of total hemoglobin (Hbt) concentration (the sum of Hbr and HbO_2 concentrations), respectively. This is because at 620 nm, the absorption coefficient of Hbr is about 10 times larger than that of HbO_2 and 569 nm corresponds to the isosbestic point of Hbr and HbO_2 absorption (Fig. 1 inset). In addition, we recorded intrinsic signals at 538 nm, where HbO_2 has a higher absorption coefficient than Hbr. Figure 3*A* shows

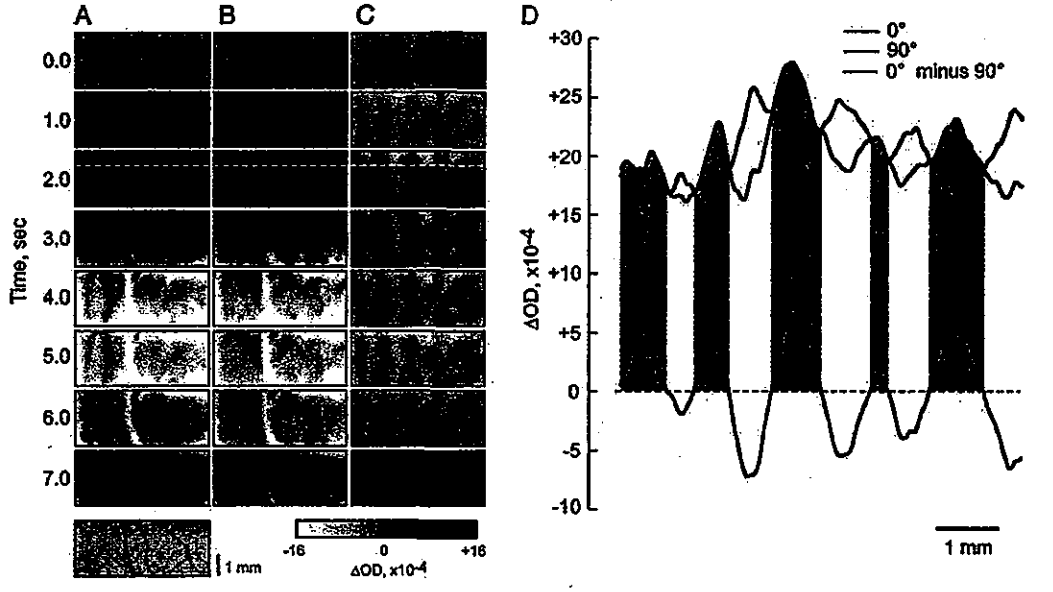

Figure 2. Stimulus-specific and stimulus-nonspecific components of intrinsic signals. (*A, B*) Images of intrinsic signal at 620 nm induced by gratings with 0° (*A*) and 90° (*B*) orientations along with the ROI at the bottom (cortical surface image taken at 538 nm). Grayscale range is shown at the bottom. The images are shown as a function of time from the stimulus onset. The stimulus duration was 2 s. (*C*) Differential images obtained by subtracting images in *B* from images in *A*. Black and white patches were specific to gratings of 0° and 90° orientations respectively. (*D*) Magnitudes of signal intensities along white broken lines on the images (*A–C*) at 2.0 s after stimulus onset. The horizontal broken line indicates the baseline corresponding to the absence of absorption change. Shaded regions indicate the portions showing larger responses to a grating at 0° orientation. The high-frequency noise of the lines was removed using the high-cut filter (*cutoff frequency* σ = 10/mm).

the time courses of stimulus-nonspecific components of the intrinsic signals obtained at these wavelengths. At 620 nm, we consistently observed biphasic time courses, in which the light absorption increased after stimulus onset, reached a maximum after 2 s and decreased, going below the baseline (time to reach the minimum, 5 s). On the other hand, the time courses of the signals at 538 and 569 nm were monophasic: the light absorption increased and returned to the baseline without crossing it (time to reach the maximum, 3.5 s). In accordance with the absorption coefficients of hemoglobin at 538 and 569 nm, light absorption changes at 538 nm were slightly larger than those at 569 nm. The biphasic time course of the signal at 620 nm suggests that Hbr concentration initially increased due to oxygen consumption of activated neurons, which was followed by a decrease in Hbr concentration below the baseline due to blood inflow outstripping oxygen consumption. On the other hand, the absorption increase at 569 nm can be explained by the increase in Hbt resulting from the increase in blood inflow.

Spatial Patterns of Stimulus-specific Component of Intrinsic Signals

Unlike the stimulus-nonspecific components of the intrinsic signals, the polarity of the stimulus-specific components did not change at these wavelengths (Fig. 3*B*). Thus, to visualize the spatial patterns of the stimulus-specific components, we first temporally averaged the intrinsic signals from 1 to 7 s after stimulus onset. Then, the differential images of the signals were calculated by subtracting the temporally averaged images for one orientation from those for the orthogonal orientation (Fig. 4*A*). Even if the physiological sources of the signals seem to be different among these wavelengths, the spatial patterns of the stimulus-specific components were almost identical. The correlation coefficients between the differential images obtained at 620 nm and those at other wavelengths calculated on a pixel-by-pixel basis were significantly high (0.86 and 0.90 for the images obtained at 538 and 569 nm respectively; $P < 0.01$). We obtained consistent results for the other 13 cats: the average correlation coefficients for the 14 cats were 0.78 ± 0.08 for the images at 538 nm and 0.71 ± 0.09 for the images at 569 nm. These values indicate that there is a statistically significant correlation between differential images obtained at 620 nm and those obtained at other wavelengths ($P < 0.01$). These results indicate that the intrinsic signals recorded at these three wavelengths have a sufficient spatial resolution to resolve orientation-specific columnar organizations.

To estimate their spatial resolution quantitatively, we calculated the distance between neighboring iso-orientation domains and the size of the domains from the autocorrelation maps of differential images (see Materials and Methods). Figure 4*B* shows an example of the autocorrelation map of a differential image at 569 nm and its spatial profiles along the broken line that connects the central and adjacent peaks. In this example, the distance between neighboring iso-orientation domains was estimated to be 1.38 mm from the profile, and the full width at half-maximum (FWHM) of the profile's central peak was 0.65 mm. The average spatial separation between iso-orientation domains for the 14 cats was 1.34 ± 0.29 mm, and the average FWHM was 0.58 ± 0.12 mm (mean ± SD). Accordingly,

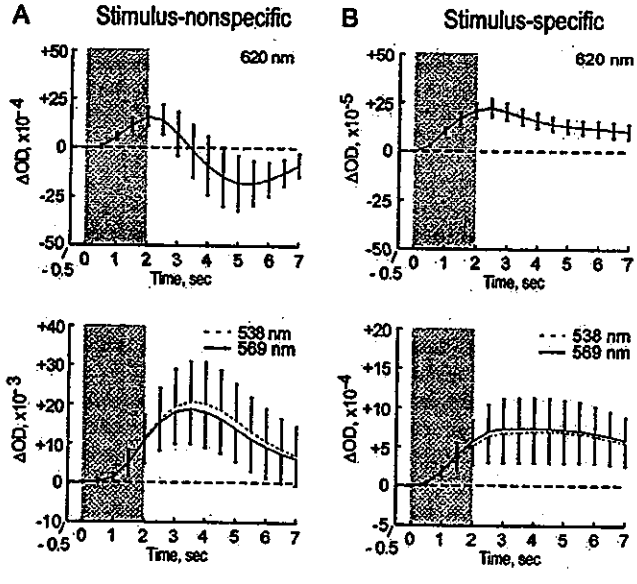

Figure 3. Time courses of stimulus-nonspecific and stimulus-specific components of intrinsic signals. (*A*) Time courses of intrinsic signals for stimulus-nonspecific components. Upper panel: 620 nm, Lower panel: 538 nm (dotted line) and 569 nm (solid line). (*B*) Time courses of intrinsic signals for stimulus-specific components. Upper panel: 620 nm, Lower panel: 538 nm (dotted line) and 569 nm (solid line). Error bars indicate one standard deviation (SD) of mean obtained from 14 cats. The shaded region indicates the duration of stimulus presentation. The horizontal broken line indicates the baseline corresponding to no absorption change.

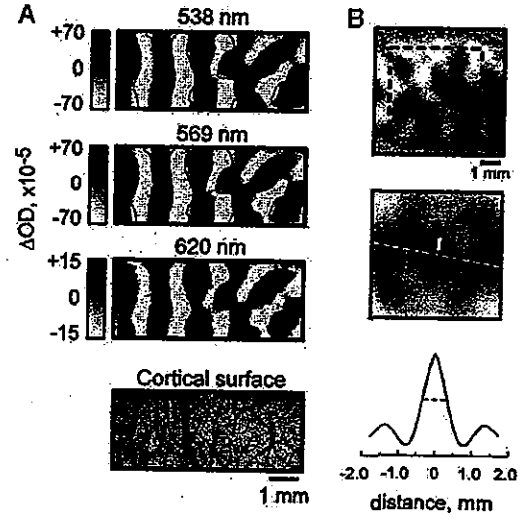

Figure 4. Spatial patterns of stimulus-specific components of intrinsic signals. (*A*) Differential images obtained from intrinsic signals at three wavelengths. The images were obtained by subtracting the responses to a grating at 90° orientation from those to a grating at 0° orientation. Black and white patches are specific to gratings at 0° and 90° orientations, respectively. Borders between active and less-active domains at 620 nm (red lines) are superimposed on each panel. This result and the result in Figure 2 were obtained from the same cortical ROI. (*B*) The analysis of spatial separations of neighboring iso-orientation domains and the domain sizes. Top panel: a differential image at 569 nm, where black and white patches are specific to gratings at 0° and 90° orientations, respectively. The grayscale range of ΔOD is $\pm 3.7 \times 10^{-4}$. The dotted rectangle (3.5 × 3.5 mm^2) in the differential image indicates the ROI for the analysis. Middle panel: the autocorrelation map of the ROI. White and black arrows indicate the largest peak (central peak) and secondary largest peaks on the map, respectively. Bottom panel: the spatial profile of the autocorrelation map along the broken line in the middle panel. The horizontal broken line in this profile indicates the FWHM of the central peak.